Necrosulfonamide causes ubiquitination of PCM1 and impairs Ciliogenesis and Autophagy

Carolina Alves Nicolau[1,2], Clotilde C.N. Renaud[1,2+], Clément Maghe[1,2+], Kilian Trillet[1,2], Jane Jardine[1,2], Sophie Escot[4], Nicolas David[4], Julie Gavard[1,2,3], Nicolas Bidère[1,2,5,*]

[1] Team SOAP, CRCI[2]NA, Nantes University, INSERM, CNRS, Université d'Angers, Nantes, France
[2] Equipe Labellisée Ligue Contre le Cancer, Paris, France
[3] Institut de Cancérologie de l'Ouest (ICO), Saint-Herblain, France
[4] Laboratoire d'Optique et de Biosciences LOB, Ecole Polytechnique, Palaiseau, France
[+] equally contribution
[5] Lead Contact
[*] Correspondence: nicolas.bidere@inserm.fr

Summary
Centriolar satellites are high-order assemblies, scaffolded by the Pericentriolar Material 1 (PCM1) protein, that gravitate as particles around the centrosome. Centriolar satellites have been linked to key cellular processes including the formation of primary cilia and GABARAP-mediated autophagy. However, to date, there is no pharmacological inhibitor of centriolar satellites. Here, we report that necrosulfonamide (NSA), a compound previously shown to target the cell death effector MLKL, induced non-degradative ubiquitination of PCM1. This also caused a defect in ciliogenesis and an accumulation of autophagy markers such as P62 and GABARAPL1, although the overall architecture and distribution of centriolar satellites were maintained. We further found that the depletion of PCM1 lessened the impact of NSA on autophagy. Altogether, NSA may be a valuable tool to study centriolar satellites and provide further insights into their interplay with autophagy.

Keywords: Necrosulfonamide, centriolar satellites, PCM1, primary cilia, autophagy, GABARAP, P62

Introduction

Centriolar satellites are small membrane-less electron-dense particles of 70-100 nm in diameter that concentrate around the centrosome [1–3]. Pericentriolar Material 1(PCM1) protein, the founding member of centriolar satellites, scaffolds these structures [4,5]. Recent omics studies identified >200 proteins bound to PCM1 and >600 proteins in the interactome of 22 satellite components, among which 40% are shared with the centrosome interactome, illustrating the composite, dynamic, and complex nature of centriolar satellites [6,7]. A large body of work now supports a role for centriolar satellites in the formation of primary cilia, a microtubule-based organelle that protrudes from the cell body, senses and integrates extracellular signals to regulate cell proliferation, polarity, nerve growth, differentiation, or tissue maintenance [8,9]. Notably, mutations in genes encoding centriolar satellite components lead to defects in ciliogenesis and cause a variety of diseases and syndromes termed ciliopathies [10]. Accordingly, the depletion of PCM1 disrupts centriolar satellites and prevents the formation of primary cilia [11–13]. Nonetheless, centriolar satellites also exert functions beyond ciliogenesis, such as centrosome homeostasis maintenance, microtubule organization, aggresome clearance, stress response, neurogenesis, and autophagy [12,14–20]. For instance, PCM1 binds and prevents the autophagy regulator GABARAP from proteasomal degradation, thereby regulating the maturation of autophagosome [17,18,21].

PCM1 is tightly regulated by subcellular location and post-translational modifications (PTMs) [2]. For instance, PCM1 is redistributed in the cytosol of the cells during mitosis or when microtubules are dismantled, and in cells exposed to cellular stresses such as UV radiation, heat shock, and transcription block [4,22,23]. PCM1 is also differentially phosphorylated during the cell cycle. Accordingly, the phosphorylation of PCM1 by the polo-like kinase 4 (PLK4) on its serine residue 372 during the G1 phase is crucial for its dimerization and the maintenance of centriolar satellites [24]. By contrast, the phosphorylation of PCM1 at T^{703} by the Cyclin-dependent kinase 1 (CDK1) during the transition from the G2 phase to mitosis leads to the dismantlement of centriolar satellites [25]. Moreover, PCM1 is also marked by ubiquitin chains, catalyzed by the E3-ligase Mindbomb 1 (MIB1), and this leads to proteasomal degradation and, thereby, disruption of centriolar satellites [11,13,22]. By trimming these ubiquitin chains, the deubiquitin enzyme (DUB) Ubiquitin Specific Peptidase 9 X-Linked (USP9X) limits the degradation of PCM1 [26,27].

In this work, we show that the small molecule necrosulfonamide (NSA), a known inhibitor of cell death by necroptosis [28], drives the non-degradative ubiquitination of PCM1. Although the structure of centriolar satellites is maintained, NSA blocks ciliogenesis and causes an accumulation of the autophagy markers P62 (SQSTM1) and GABARAPL1, at both RNA and protein levels. Furthermore, we observed that the effects of NSA on autophagy partly rely on PCM1. Together, these results identify NSA as a new valuable tool to study centriolar satellites and provide new insights into the interplay between centriolar satellites and autophagy.

Results and Discussion

Necrosulfonamide triggers the Ubiquitination of PCM1.

In order to identify novel compounds prone to altering PCM1 status and/or abundance, we devised a screen by immunoblotting analysis of a panel of 35 broadly used small molecules (Fig. 1A and Table S1). The best hit was necrosulfonamide (NSA), a chemical previously shown to inhibit mixed lineage kinase domain-like pseudokinase (MLKL), a crucial effector of cell death by necroptosis and extracellular vesicles biogenesis [28–30]. When applied at non-toxic concentrations, NSA led to the appearance of slower migration species of PCM1 combined with a decrease of full-length PCM1 (Fig. 1B, 1C, and S1A-G). Although the level of the centriolar satellite component CEP131 was also diminished, the abundance in several other PCM1 partners remained unchanged (Fig. 1C). Further militating against a global degradation of PCM1, PCM1 efficiently co-immunoprecipitated with its known partners CEP290, MIB1, and CEP131, and is normally distributed around the centrosome in the presence of NSA (Fig. 1D and 1E). At the mRNA level, we found that NSA did not overtly affect PCM1 and other centriolar satellite components except CEP131 in Jurkat T cells (Fig. S1H). By contrast, NSA increased PCM1 but not CEP131 mRNA levels in RPE-1 cells, suggesting cell-type specific changes (see below, Fig. S3K). Hence, PCM1 is biochemically modified by NSA but retains its ability to interact with its partners and to organize spatially in cells.

These PTMs of PCM1 in the presence of NSA evoke ubiquitination. Supporting this idea, the selective pull-down of endogenous proteins marked with ubiquitin with tandem ubiquitin-binding entities (TUBE) showed that NSA drives PCM1 ubiquitination (Fig. 1F). MIB1 has been shown to stamp ubiquitin chains onto PCM1 and thereby, to drive its proteasomal degradation [11,13,22]. Yet, slow-migration species of PCM1 were not further increased by the addition of the proteasome inhibitor MG132 (Fig. 1G). In addition, the siRNA-based

depletion of MIB1 had no effect on the modification of PCM1 induced by NSA (Fig. S1I). This was also true when the DUB USP9X, which counteracts MIB1-dependent ubiquitination of PCM1 [27], was silenced, suggesting MIB1-independent ubiquitination (Fig. S1J). Altogether, this suggests that NSA drives the ubiquitination of PCM1.

Necrosulfonamide impacts PCM1 and Ciliogenesis independently of MLKL

Because PCM1 is instrumental for ciliogenesis [12], we next assessed the impact of NSA on the formation of primary cilia in serum-starved retinal-pigmented epithelial (RPE-1) cells. We found that NSA led to a significant reduction in the number of cells forming primary cilia (Fig. 2A and 2B). These data suggest that NSA impairs ciliogenesis.

NSA was previously shown to bind the Cysteine in position 86 of human MLKL and, thereby, blocks its oligomerization and subsequent programmed cell death by necroptosis [28]. A streptavidin pull-down of cell lysates treated with biotinylated NSA showed that both endogenous and GFP-tagged PCM1 can bind to NSA and endogenous MLKL (Fig. S2A and S2B). As expected, this binding was reduced by the addition of cold competitive NSA, as previously shown for MLKL [28]. This suggests that PCM1 may be a new target for NSA. In mouse MLKL, the Cys^{86} is substituted with a Tryptophan residue, making NSA inefficient [28]. Nevertheless, we observed that NSA also modified PCM1 in mouse (L929, MEFs) cell lines (Fig. 2C, and S2C), suggesting an MLKL-independent action. Accordingly, NSA hampered serum starvation-induced ciliogenesis in MEFs (Fig. 2D and 2E). Lastly, MLKL was targeted with small interfering RNA (siRNA) in RPE-1 cells. Again, NSA-mediated PCM1 PTMs occurred normally (Fig. 2F). In addition, MLKL silencing had no overt impact on ciliogenesis induced by serum starvation or on the ability of NSA to prevent it (Fig. 2G and 2H). Altogether, this suggests that NSA alters PCM1 in an MLKL-independent manner.

Necrosulfonamide leads to Defects in Autophagy

To gain insights into the signaling pathways impaired by NSA treatment, we next carried out a transcriptomic analysis by RNAseq of Jurkat cells treated overnight with NSA. This identified 3,875 genes up-regulated in NSA 2.5 µM condition, out of which 134 were enriched with a False discovery rate (FDR) <25% (Fig. S3A). The gene set enrichment analysis (GSEA) indicated that the transition from G2 to mitosis and the proteasomal ubiquitin-dependent process were some of the most impacted pathways upon NSA treatment (Fig. S3B). The assembly of centriolar satellites, as well as the turnover of their proteins, are tightly controlled during the cell cycle and by proteasome degradation [2]. Additionally, the functional analysis of the differentially expressed genes in NSA condition showed that biological processes such as the Wnt pathway, cell fate, and neuron differentiation, which have been linked with ciliogenesis [31,32], were also impaired (Fig. S3C). This gene functional analysis supports the effect of NSA on ciliogenesis herein observed.

In addition to proteasome-related processes, other proteostasis signatures including macroautophagy and lysosome were identified (Fig. 3A). The screen of a qPCR-based array of autophagy regulators revealed an up-regulation of some autophagy markers, including GABARAPL1 and SQSTM1 (P62) in NSA-treated cells (Fig. 3B). The increase in GABARAPL1 and P62 levels in response to NSA treatment, was further confirmed at the protein levels by immunofluorescence in basal autophagy condition (Fig. 3C). The same was true during autophagy induced by starvation, whether or not human and mouse cell lines were refed (Fig. 3D, S3D, and S3E). Of note, the inhibition of autophagy with the V-ATPase inhibitors Bafilomycin A1 did not interfere with the action of NSA on PCM1 nor on P62 and

GABARAPL1 (Fig. S3F). Lastly, we found that the autophagy defects caused by NSA were mostly independent of MLKL and occurred in mouse cell lines (Fig. 3E, and S3G).

The transcription factor EB (TFEB) is a master regulator of genes involved in the different steps of autophagy, including SQSTM1 (P62), MAP1LC3B, or GABARAP [33,34]. We observed that TFEB depletion by siRNA reduced the NSA-driven induction of GABARAPL1 (Fig. S3H). To test if NSA targets the early stages of autophagy, we next silenced Beclin1, a key regulator of autophagosome nucleation and maturation [35]. However, no significant changes were observed (Figure S3I). Hence, NSA leads to an accumulation of some of the autophagy markers at RNA and protein levels without completely interfering with autophagy.

PCM1 interacts with GABARAPL1 via an LC3-interacting region (LIR) motif and regulates autophagy [18]. Thus, we wondered whether NSA drives PCM1 PTMs and alteration of autophagy markers in a linear manner or independently. First, we observed that NSA-driven PCM1 PTMs precede the accumulation of P62, and GABARAPL1 (Fig. 3F and 3G). Next, GABARAPL1 was silenced with siRNA. This was accompanied by an increase in the abundance of autophagy markers at RNA and protein levels (Fig. 3H and S3J). However, the components of centriolar satellites remained mostly unchanged, with the exception of CEP55 and CYLD (Fig. S3J). Importantly, the treatment with NSA normally led to PCM1 PTMs and to a potent increase in P62 abundance (Fig. 3H). Lastly, the impact of PCM1 on NSA-mediated upregulation of GABARAPL1 and P62 was assessed. Although we observed an increase in the abundance of P62 and GABARAPL1 in RPE-1 cells without PCM1, it was not further strongly enhanced by NSA (Fig. 3H, and S3K). Of note, the binding between PCM1 and GABARAPL1 was not changed in cells treated with NSA (Fig. S3L). Taken together, these results suggest that the accumulation of autophagy markers induced by NSA treatment partially depends on PCM1.

Centriolar satellites have been shown to participate in key cellular functions including ciliogenesis, autophagy, clearance of pathogenic aggregates containing misfolded proteins, microtubule organization, and neurogenesis [2]. The vast majority of the work dealing with centriolar satellites is based on the genetic depletion of the scaffold PCM1, which disrupts the architecture of these structures and, to date, no chemical inhibitors have been described. We now report that NSA interferes with centriolar satellite functions in human and murine cells *in vitro* without affecting their assembly or their spatial location in cells. Although additional work will be required to test all known functions linked with the centriolar satellites, we show that NSA causes a defect in autophagy and inhibits the formation of primary cilia induced by starvation. NSA might therefore be a valuable tool to validate and expand our understanding of the cellular processes controlled by the centriolar satellites.

How exactly NSA inhibits centriolar satellites remains unclear. NSA is an alkylating agent likely targeting cysteine residues, that was initially found to bind to the Cys^{86} of human MLKL [28]. This disrupts disulfide bonds formed by MLKL and thereby prevents MLKL oligomerization and insertion in the plasma membrane, a key step in the execution of necroptosis [28]. More recently, NSA was also shown to limit cell death by pyroptosis [36,37], and this partly results from the direct binding to the Cys^{191} of the pore-forming protein Gasdermin D (GSDMD) [36]. Although we conclusively showed that NSA binds to PCM1, additional work is required to establish whether this interaction is direct. Because NSA drives the attachment of polyubiquitin chains onto PCM1, it could also enhance the activity of an E3 ligase or inhibit the one of a deubiquitin enzyme. Nevertheless, our work further illustrates how post-translational modifications of PCM1 tightly regulate its function [2]. Hence, strategies aimed at

targeting PCM1 ubiquitination status might be relevant to fine-tuning the activities of centriolar satellites.

Limitations of the Study

Our study indicates that NSA drives PCM1 ubiquitination and alters cellular functions downstream of PCM1 such as primary cilia formation and stability of autophagy regulators. However, we have not formally demonstrated the link between these observations. For instance, whether and how PCM1 ubiquitination remodels centriolar satellites from a molecular standpoint remains to be tested. Future studies will therefore be required to identify the residues stamped with polyubiquitin chains and the impact of this modification on the functions controlled by PCM1.

Resource Availability

Lead Contact

Further information and requests for resources and reagents should be directed to and will be fulfilled by the Lead Contact, Nicolas Bidère (nicolas.bidere@inserm.fr).

Materials Availability

All reagents generated in this study are available from the Lead Contact with a completed Material Transfer Agreement.

Data and Code Availability

This study did not generate large-scale datasets. Raw data of this article are available from the Lead Contact upon request.

Methods

All methods can be found in the accompanying Transparent Methods supplemental file.

Supplemental Information

Supplemental information can be found online at https://doi.org/XXXXX

Acknowledgments

We thank Sylvie Urbé (The University of Liverpool) and Takashi Toda (Hiroshima University) for kindly providing reagents as well as the MicroPicell facility (SFR Santé François Bonamy, Nantes, France) for the expertise and discussions for imaging analysis. This work was funded by an International Program for Scientific Cooperation (PICS, CNRS), Fondation de France, Fondation pour la Recherche Médicale (Equipe labellisée DEQ20180339184), Fondation ARC contre le Cancer (PJA to J.G. and N.B.), Institut National du Cancer (INCa PLBIO 2019-151, INCa PLBIO 2019-291, INCa PAIR-CEREB lNCa_16285), Ligue nationale contre le cancer (Equipe labellisée) et comités de Loire-Atlantique, Maine et Loire, Vendée, Ille-et-Vilaine (J.G., N.B.). C.A.N. received a fellowship from Fondation de France, C.C.N.R. from INSERM and Région Pays de la Loire, C.M. from Ligue Régionale contre le Cancer and Région Pays-de-la-Loire, and J.J. from Fondation pour la Recherche Médicale. The team is part of the SIRIC ILIAD (INCA-DGOS-Inserm_12558).

Author Contributions

Conceptualization, C.A.N., C.C.N.R., C.M., K.T., J.J., S.E., N.D., J.G., and N.B.; Methodology, C.A.N., C.C.N.R., C.M., K.T., and J.J.; Investigation, C.A.N., C.C.N.R., C.M., K.T., and J.J.; Supervision: N.B.; Writing-Original Draft, C.A.N., and N.B.; Writing-Review and Editing, C.A.N., C.C.N.R., C.M., K.T., J.J., J.G., and N.B.; Funding Acquisition, J.G., and N.B.

Declaration of interests

The authors declare no competing interests.

References

1. Prosser, S.L., and Pelletier, L. (2020). Centriolar satellite biogenesis and function in vertebrate cells. Journal of Cell Science *133*, jcs239566. 10.1242/jcs.239566.
2. Renaud, C.C.N., and Bidère, N. (2021). Function of Centriolar Satellites and Regulation by Post-Translational Modifications. Front Cell Dev Biol *9*, 780502. 10.3389/fcell.2021.780502.
3. Odabasi, E., Batman, U., and Firat-Karalar, E.N. (2020). Unraveling the mysteries of centriolar satellites: time to rewrite the textbooks about the centrosome/cilium complex. Mol Biol Cell *31*, 866–872. 10.1091/mbc.E19-07-0402.
4. Dammermann, A., and Merdes, A. (2002). Assembly of centrosomal proteins and microtubule organization depends on PCM-1. J Cell Biol *159*, 255–266. 10.1083/jcb.200204023.
5. Balczon, R., Bao, L., and Zimmer, W.E. (1994). PCM-1, A 228-kD centrosome autoantigen with a distinct cell cycle distribution. J Cell Biol *124*, 783–793. 10.1083/jcb.124.5.783.
6. Quarantotti, V., Chen, J.-X., Tischer, J., Gonzalez Tejedo, C., Papachristou, E.K., D'Santos, C.S., Kilmartin, J.V., Miller, M.L., and Gergely, F. (2019). Centriolar satellites are acentriolar assemblies of centrosomal proteins. EMBO J *38*, e101082. 10.15252/embj.2018101082.
7. Gheiratmand, L., Coyaud, E., Gupta, G.D., Laurent, E.M., Hasegan, M., Prosser, S.L., Gonçalves, J., Raught, B., and Pelletier, L. (2019). Spatial and proteomic profiling reveals centrosome-independent features of centriolar satellites. EMBO J *38*, e101109. 10.15252/embj.2018101109.
8. Malicki, J.J., and Johnson, C.A. (2017). The Cilium: Cellular Antenna and Central Processing Unit. Trends Cell Biol *27*, 126–140. 10.1016/j.tcb.2016.08.002.
9. Hildebrandt, F., Benzing, T., and Katsanis, N. (2011). Ciliopathies. N Engl J Med *364*, 1533–1543. 10.1056/NEJMra1010172.
10. Hori, A., and Toda, T. (2017). Regulation of centriolar satellite integrity and its physiology. Cell Mol Life Sci *74*, 213–229. 10.1007/s00018-016-2315-x.
11. Wang, L., Lee, K., Malonis, R., Sanchez, I., and Dynlacht, B.D. (2016). Tethering of an E3 ligase by PCM1 regulates the abundance of centrosomal KIAA0586/Talpid3 and promotes ciliogenesis. Elife *5*, e12950. 10.7554/eLife.12950.
12. Odabasi, E., Gul, S., Kavakli, I.H., and Firat-Karalar, E.N. (2019). Centriolar satellites are required for efficient ciliogenesis and ciliary content regulation. EMBO Rep *20*, e47723. 10.15252/embr.201947723.
13. Douanne, T., André-Grégoire, G., Thys, A., Trillet, K., Gavard, J., and Bidère, N. (2019). CYLD Regulates Centriolar Satellites Proteostasis by Counteracting the E3 Ligase MIB1. Cell Rep *27*, 1657-1665.e4. 10.1016/j.celrep.2019.04.036.
14. Ge, X., Frank, C.L., Calderon de Anda, F., and Tsai, L.-H. (2010). Hook3 interacts with PCM1 to regulate pericentriolar material assembly and the timing of neurogenesis. Neuron *65*, 191–203. 10.1016/j.neuron.2010.01.011.
15. Pampliega, O., Orhon, I., Patel, B., Sridhar, S., Díaz-Carretero, A., Beau, I., Codogno, P., Satir, B.H., Satir, P., and Cuervo, A.M. (2013). Functional interaction between autophagy and ciliogenesis. Nature *502*, 194–200. 10.1038/nature12639.
16. Tang, Z., Lin, M.G., Stowe, T.R., Chen, S., Zhu, M., Stearns, T., Franco, B., and Zhong, Q. (2013). Autophagy promotes primary ciliogenesis by removing OFD1 from

centriolar satellites. Nature *502*, 254–257. 10.1038/nature12606.
17. Holdgaard, S.G., Cianfanelli, V., Pupo, E., Lambrughi, M., Lubas, M., Nielsen, J.C., Eibes, S., Maiani, E., Harder, L.M., Wesch, N., et al. (2019). Selective autophagy maintains centrosome integrity and accurate mitosis by turnover of centriolar satellites. Nat Commun *10*, 4176. 10.1038/s41467-019-12094-9.
18. Joachim, J., Razi, M., Judith, D., Wirth, M., Calamita, E., Encheva, V., Dynlacht, B.D., Snijders, A.P., O'Reilly, N., Jefferies, H.B.J., et al. (2017). Centriolar Satellites Control GABARAP Ubiquitination and GABARAP-Mediated Autophagy. Curr Biol *27*, 2123-2136.e7. 10.1016/j.cub.2017.06.021.
19. Prosser, S.L., Tkach, J., Gheiratmand, L., Kim, J., Raught, B., Morrison, C.G., and Pelletier, L. (2022). Aggresome assembly at the centrosome is driven by CP110-CEP97-CEP290 and centriolar satellites. Nat Cell Biol *24*, 483–496. 10.1038/s41556-022-00869-0.
20. Wang, L., Paudyal, S.C., Kang, Y., Owa, M., Liang, F.-X., Spektor, A., Knaut, H., Sánchez, I., and Dynlacht, B.D. (2022). Regulators of tubulin polyglutamylation control nuclear shape and cilium disassembly by balancing microtubule and actin assembly. Cell Res *32*, 190–209. 10.1038/s41422-021-00584-9.
21. Martello, A., Lauriola, A., Mellis, D., Parish, E., Dawson, J.C., Imrie, L., Vidmar, M., Gammoh, N., Mitić, T., Brittan, M., et al. (2020). Trichoplein binds PCM1 and controls endothelial cell function by regulating autophagy. EMBO Rep *21*, e48192. 10.15252/embr.201948192.
22. Villumsen, B.H., Danielsen, J.R., Povlsen, L., Sylvestersen, K.B., Merdes, A., Beli, P., Yang, Y.-G., Choudhary, C., Nielsen, M.L., Mailand, N., et al. (2013). A new cellular stress response that triggers centriolar satellite reorganization and ciliogenesis. EMBO J *32*, 3029–3040. 10.1038/emboj.2013.223.
23. Tollenaere, M.A.X., Villumsen, B.H., Blasius, M., Nielsen, J.C., Wagner, S.A., Bartek, J., Beli, P., Mailand, N., and Bekker-Jensen, S. (2015). p38- and MK2-dependent signalling promotes stress-induced centriolar satellite remodelling via 14-3-3-dependent sequestration of CEP131/AZI1. Nat Commun *6*, 10075. 10.1038/ncomms10075.
24. Hori, A., Barnouin, K., Snijders, A.P., and Toda, T. (2016). A non-canonical function of Plk4 in centriolar satellite integrity and ciliogenesis through PCM1 phosphorylation. EMBO Rep *17*, 326–337. 10.15252/embr.201541432.
25. Wang, G., Chen, Q., Zhang, X., Zhang, B., Zhuo, X., Liu, J., Jiang, Q., and Zhang, C. (2013). PCM1 recruits Plk1 to the pericentriolar matrix to promote primary cilia disassembly before mitotic entry. J Cell Sci *126*, 1355–1365. 10.1242/jcs.114918.
26. Li, X., Song, N., Liu, L., Liu, X., Ding, X., Song, X., Yang, S., Shan, L., Zhou, X., Su, D., et al. (2017). USP9X regulates centrosome duplication and promotes breast carcinogenesis. Nat Commun *8*, 14866. 10.1038/ncomms14866.
27. Han, K.-J., Wu, Z., Pearson, C.G., Peng, J., Song, K., and Liu, C.-W. (2019). Deubiquitylase USP9X maintains centriolar satellite integrity by stabilizing pericentriolar material 1 protein. J Cell Sci *132*, jcs221663. 10.1242/jcs.221663.
28. Sun, L., Wang, H., Wang, Z., He, S., Chen, S., Liao, D., Wang, L., Yan, J., Liu, W., Lei, X., et al. (2012). Mixed lineage kinase domain-like protein mediates necrosis signaling downstream of RIP3 kinase. Cell *148*, 213–227. 10.1016/j.cell.2011.11.031.
29. Yoon, S., Kovalenko, A., Bogdanov, K., and Wallach, D. (2017). MLKL, the Protein that Mediates Necroptosis, Also Regulates Endosomal Trafficking and Extracellular Vesicle Generation. Immunity *47*, 51-65.e7. 10.1016/j.immuni.2017.06.001.
30. André-Grégoire, G., Maghe, C., Douanne, T., Rosińska, S., Spinelli, F., Thys, A., Trillet, K., Jacobs, K.A., Ballu, C., Dupont, A., et al. (2022). Inhibition of the pseudokinase MLKL alters extracellular vesicle release and reduces tumor growth in glioblastoma. iScience *25*, 105118. 10.1016/j.isci.2022.105118.

31. Avasthi, P., and Marshall, W.F. (2012). Stages of ciliogenesis and regulation of ciliary length. Differentiation *83*, S30-42. 10.1016/j.diff.2011.11.015.
32. Wheway, G., Nazlamova, L., and Hancock, J.T. (2018). Signaling through the Primary Cilium. Front. Cell Dev. Biol. *6*, 8. 10.3389/fcell.2018.00008.
33. Palmieri, M., Impey, S., Kang, H., di Ronza, A., Pelz, C., Sardiello, M., and Ballabio, A. (2011). Characterization of the CLEAR network reveals an integrated control of cellular clearance pathways. Hum Mol Genet *20*, 3852–3866. 10.1093/hmg/ddr306.
34. Settembre, C., Di Malta, C., Polito, V.A., Garcia Arencibia, M., Vetrini, F., Erdin, S., Erdin, S.U., Huynh, T., Medina, D., Colella, P., et al. (2011). TFEB links autophagy to lysosomal biogenesis. Science *332*, 1429–1433. 10.1126/science.1204592.
35. Kang, R., Zeh, H.J., Lotze, M.T., and Tang, D. (2011). The Beclin 1 network regulates autophagy and apoptosis. Cell Death Differ *18*, 571–580. 10.1038/cdd.2010.191.
36. Rathkey, J.K., Zhao, J., Liu, Z., Chen, Y., Yang, J., Kondolf, H.C., Benson, B.L., Chirieleison, S.M., Huang, A.Y., Dubyak, G.R., et al. (2018). Chemical disruption of the pyroptotic pore-forming protein gasdermin D inhibits inflammatory cell death and sepsis. Sci Immunol *3*, eaat2738. 10.1126/sciimmunol.aat2738.
37. Rashidi, M., Simpson, D.S., Hempel, A., Frank, D., Petrie, E., Vince, A., Feltham, R., Murphy, J., Chatfield, S.M., Salvesen, G.S., et al. (2019). The Pyroptotic Cell Death Effector Gasdermin D Is Activated by Gout-Associated Uric Acid Crystals but Is Dispensable for Cell Death and IL-1β Release. J Immunol *203*, 736–748. 10.4049/jimmunol.1900228.

Figure Legends

Figure 1. Necrosulfonamide leads to the Ubiquitination of PCM1

(**A**) Densitometric measurement of PCM1 abundance, normalized to GAPDH and compared to DMSO-treated samples analyzed by Western blotting in Jurkat cells treated overnight with 35 small-molecule compounds.

(**B**) Cell lysates from Jurkat cells treated with NSA (2.5 μM), QVD (10 μM), zVAD (20 μM), Nec-1s (20 μM) or with DMSO overnight were analyzed by Western blotting with antibodies specific for the indicated proteins. Molecular weight markers (*Mr*) are indicated.

(**C**) Jurkat cells were treated with NSA (1.5 μM) overnight and analyzed as in (B). Data are representative of at least three independent experiments.

(**D**) Cell Lysates from Jurkat cells treated overnight with 2.5 μM NSA were subjected to immunoprecipitation (IP) with antibodies against PCM1, and samples were then analyzed by Western blotting as indicated. Western blots are representative of three or more independent experiments.

(**E**) Confocal microscopy analysis of RPE-1 cells treated overnight with 2.5 μM NSA showing the localization of PCM1 and γ-Tubulin, with nuclei stained by 4'-6-diamidino-2-phenylindole (DAPI). Scale bar, 5 μm. Data are representative of three independent experiments.

(**F**) Lysates from Jurkat cells treated as in (D) were subjected to a TUBE pan-ubiquitin pull-down, and analyzed by Western blotting as indicated. Data are representative of three or more independent experiments.

(**G**) RPE-1 cells were treated with NSA (2.5 and 5 μM) overnight and further incubated with 25 μM of MG132 for 3h. Cell extracts were prepared and analyzed by Western blotting with antibodies specific to the indicated proteins. The presented data are representative of two independent experiments.

Figure 2. Necrosulfonamide impacts PCM1 and Ciliogenesis independently of MLKL

(**A and B**) RPE-1 cells were serum starved and treated with 2.5 μM NSA for 24h and were then analyzed by confocal microscopy to visualize PCM1 and primary cilia (acetylated

tubulin). In (B), the histogram shows the quantification of cells with cilia (means ± SEM of three independent experiments; n > 100 cells counted per sample; ****$P < 0.0001$, ANOVA).
(**C**) Cell lysates from L929 cells treated overnight with increasing concentrations of NSA were analyzed by Western blotting with antibodies against the indicated proteins. Western blots are representative of three or more independent experiments.
(**D and E**) serum-starved MEFs cells were treated with 1.25 μM NSA or DMSO for 48h, and analyzed by confocal microscopy to visualize PCM1 and primary cilia (acetylated tubulin). Scale bar, 5 μm. The histogram shows the quantification of ciliated cells (means ± SEM of three independent experiments; n > 100 cells counted per sample; **$P < 0.01$, ANOVA).
(**F**) RPE-1 cells were transfected with small interfering RNA (siRNA) for MLKL or scramble non-specific (NS) for 48h and treated overnight with NSA as indicated. Cell extracts were prepared and analyzed by Western blotting with antibodies to the indicated proteins. Western blots are representative of three or more independent experiments.
(**G and H**) Confocal microscopy analysis of RPE-1 cells as in (F), serum-starved and treated with 2.5 μM NSA for 24h. Acetylated tubulin (cilia) and PCM1 were immunostained with specific antibodies, and nuclei were stained by DAPI. Scale bar, 5 μm. In (H), the histogram shows the quantification of ciliated cells from (means ± SEM of three independent experiments; n > 100 cells counted per sample; ****$P < 0.0001$, ANOVA). The inset blot shows the efficiency of MLKL silencing.

Figure 3. Necrosulfonamide leads to a Defect in Autophagy Signature
(**A**) RNA-seq analysis of Jurkat cells treated overnight with 2.5 μM NSA. Representation of proteostasis-related biological process identified by DAVID upon submission of the list of the differentially expressed genes in the presence of NSA.
(**B**) Volcano plot of RT^2 profiler PCR array of human autophagy signaling components for Jurkat cells treated overnight with 2.5 μM of NSA. Data represent three independent experiments. Genes up-regulated upon NSA treatment are shown in the figure.
(**C**) Confocal microscopy analysis of P62 (red) and GABARAPL1 (green) in RPE-1 cells treated overnight with 2.5 μM NSA. Bafilomycin (Baf, 100 nM) was used as a positive control. Nuclei were stained by DAPI. Scale bar, 20 μm. Data are representative of two independent experiments.
(**D**) Jurkat cells were treated overnight with 5 μM NSA followed by nutrient starvation in EBBS for 2h. When indicated, cells were reefed with either essential amino acids (AA) or complete media (Med). Cell lysates were prepared and analyzed by Western blotting with antibodies specific to the indicated proteins. Western blots are representative of three or more independent experiments.
(**E**) RPE-1 cells were transfected with small interfering RNA (siRNA) for MLKL or scramble non-specific (NS). After 48h, cells were treated overnight with 2.5 or 5 μM NSA. Cell lysates were prepared and analyzed by Western blotting with antibodies specific against the indicated proteins. Western blots are representative of three or more independent experiments.
(**F and G**) Cell lysates from Jurkat cells treated with 2.5 μM of NSA as indicated were analyzed by Western blotting with antibodies against the indicated proteins. The histograms in (G) show the densitometric analysis of P62 and GABARAPL1 (means ± SEM in comparison to DMSO, which is considered 1; ****$P < 0.0001$, ANOVA). Western blots are representative of three or more independent experiments.
(**H**) RPE-1 cells were transfected with small interfering RNA (siRNA) for PCM1, GABARAPL1, or scramble non-specific (NS). After 48h, cells were treated overnight with 2.5 or 5 μM NSA. Cell lysates were prepared and analyzed by Western blotting with antibodies specific against the indicated proteins. Western blots are representative of three or more independent experiments.

Figure 1

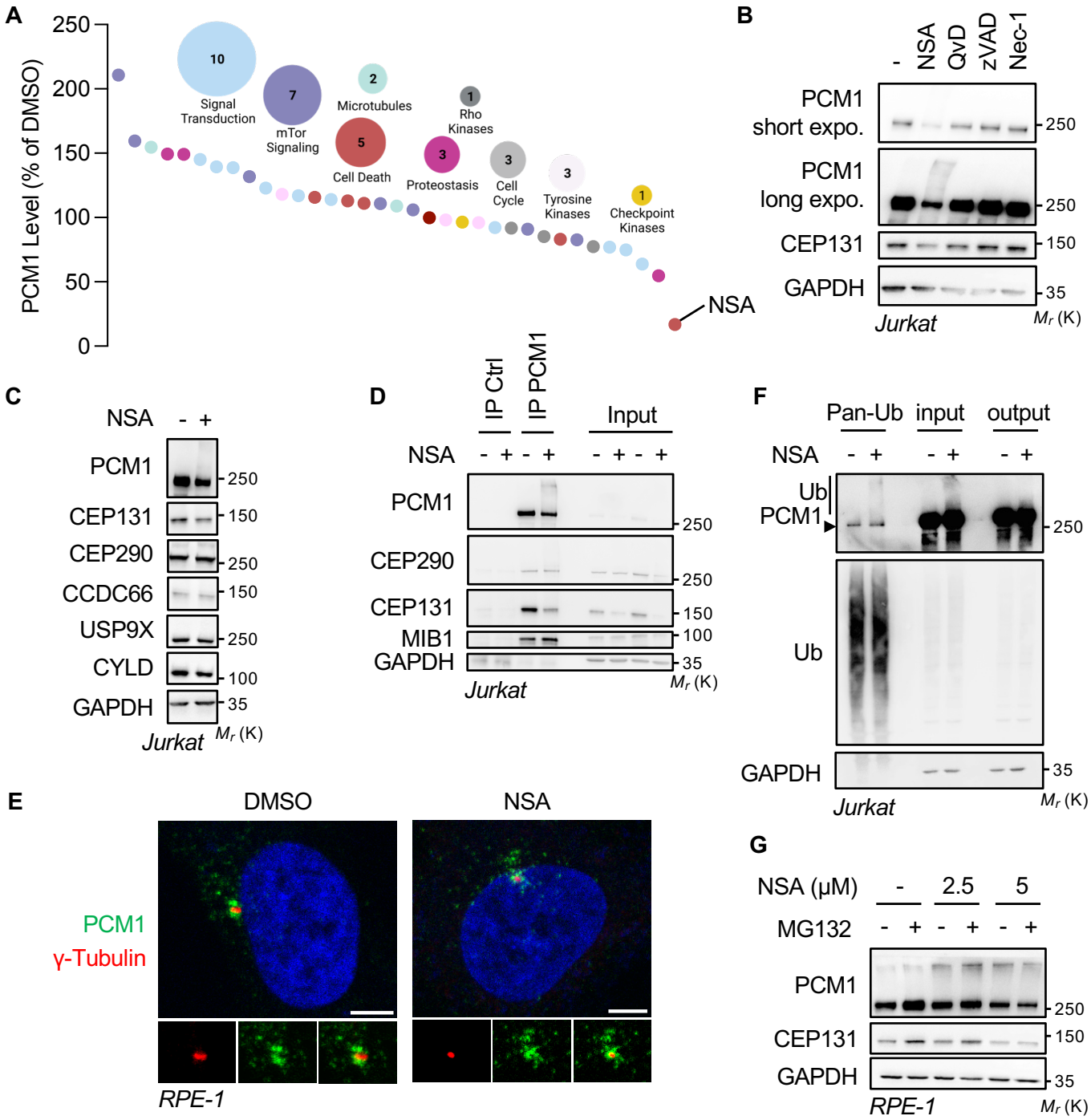
A
PCM1 Level (% of DMSO)
250
200
150
100
50
0
10
Signal Transduction
7
mTor Signaling
2
Microtubules
5
Cell Death
1
Rho Kinases
3
Proteostasis
3
Cell Cycle
3
Tyrosine Kinases
1
Checkpoint Kinases
NSA
B
-
NSA
QvD
zVAD
Nec-1
PCM1 short expo.
PCM1 long expo.
CEP131
GAPDH
250
250
150
35
Jurkat
Mr (K)
C
NSA - +
PCM1
CEP131
CEP290
CCDC66
USP9X
CYLD
GAPDH
250
150
250
150
250
100
35
Jurkat
Mr (K)
D
IP Ctrl
IP PCM1
Input
NSA - + - + - + - +
PCM1
CEP290
CEP131
MIB1
GAPDH
250
250
150
100
35
Jurkat
Mr (K)
F
Pan-Ub
input
output
NSA - + - + - +
Ub
PCM1
Ub
GAPDH
250
35
Jurkat
Mr (K)
E
DMSO
NSA
PCM1
γ-Tubulin
RPE-1
G
NSA (μM) - 2.5 5
MG132 - + - + - +
PCM1
CEP131
GAPDH
250
150
35
RPE-1
Mr (K)

Figure 2

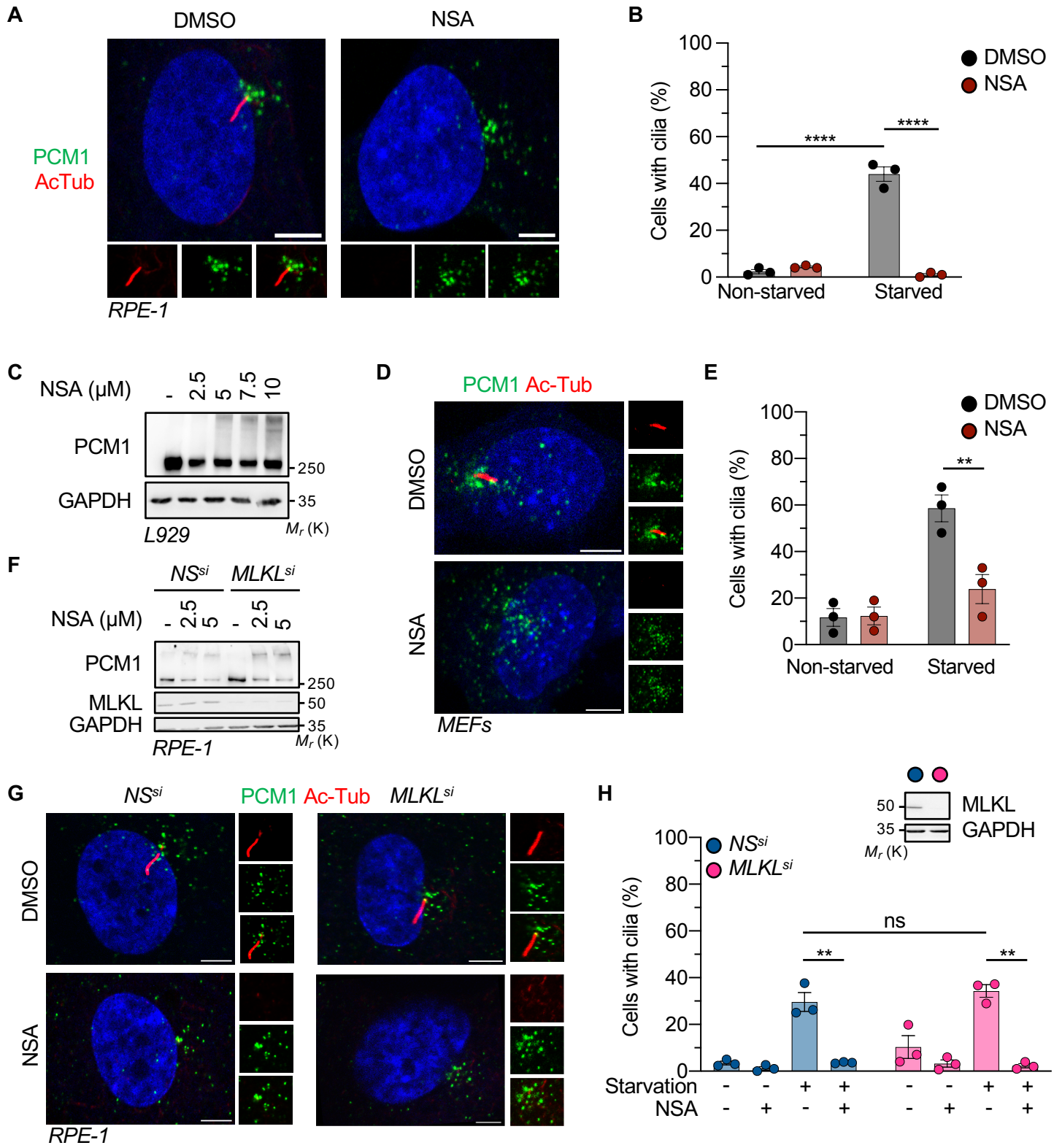
A
DMSO
NSA
PCM1
AcTub
RPE-1
B
Cells with cilia (%)
100
80
60
40
20
0
DMSO
NSA
****
****
Non-starved
Starved
C
NSA (μM)
-
2.5
5
7.5
10
PCM1
GAPDH
250
35
L929
M_r (K)
D
PCM1 Ac-Tub
DMSO
NSA
MEFs
E
Cells with cilia (%)
DMSO
NSA
**
Non-starved
Starved
F
NS^{si}
$MLKL^{si}$
NSA (μM)
-
2.5
5
-
2.5
5
PCM1
MLKL
GAPDH
250
50
35
RPE-1
M_r (K)
G
NS^{si}
PCM1 Ac-Tub
$MLKL^{si}$
DMSO
NSA
RPE-1
H
50
35
MLKL
GAPDH
M_r (K)
NS^{si}
$MLKL^{si}$
Cells with cilia (%)
ns
**
**
Starvation
NSA

Figure 3

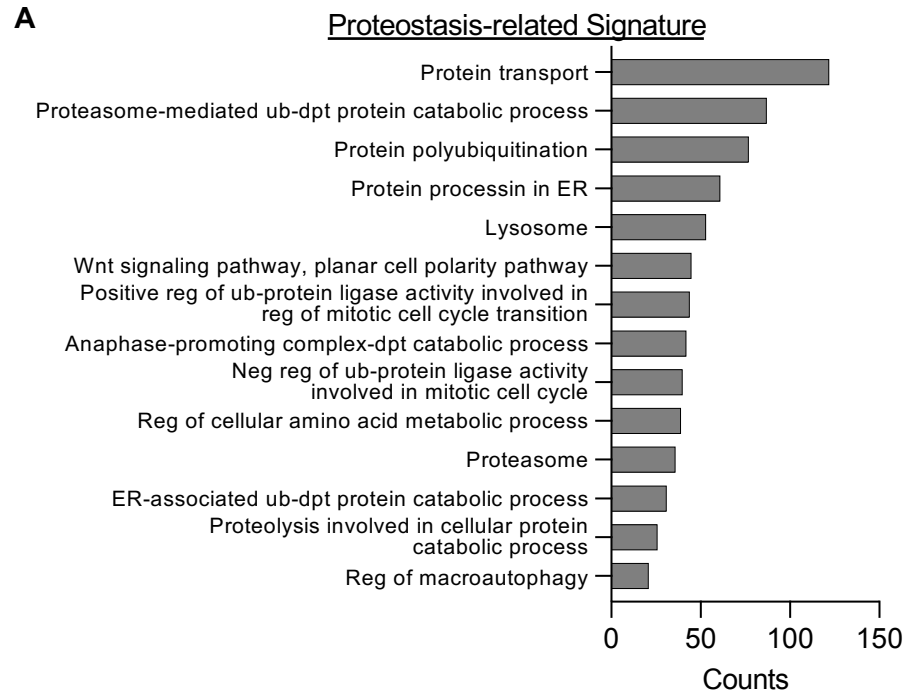

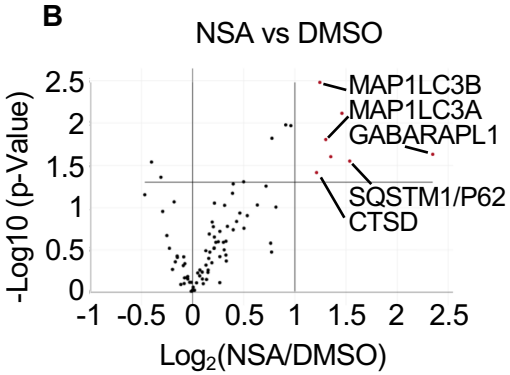
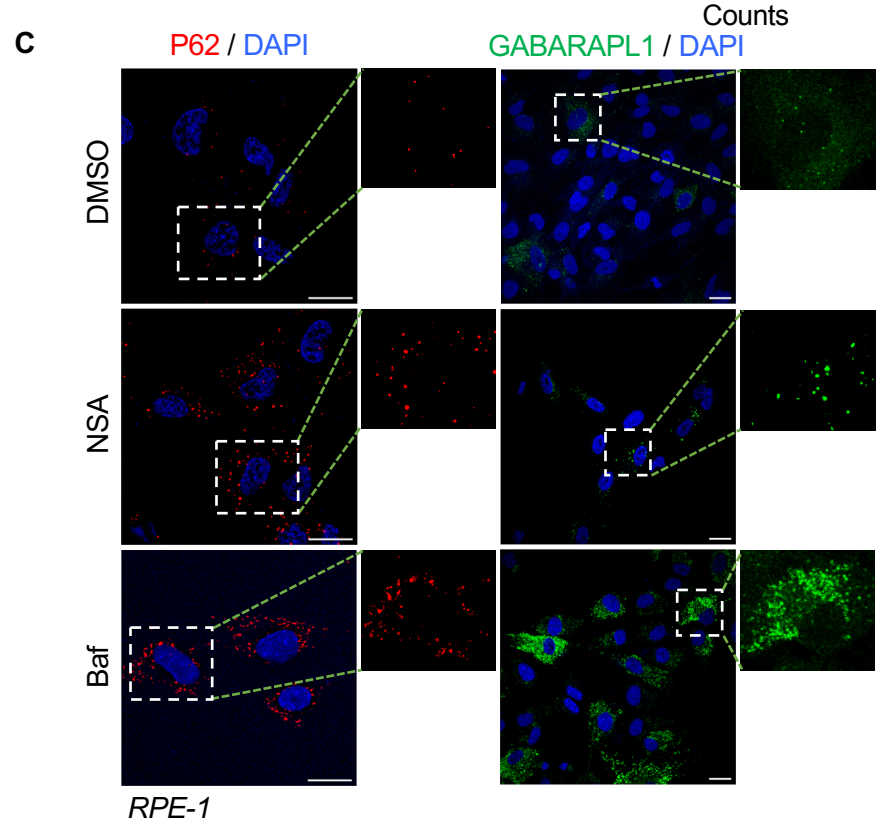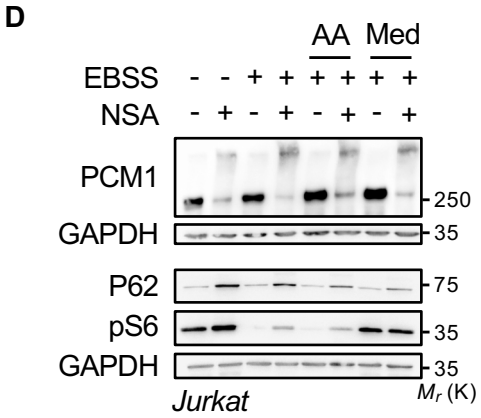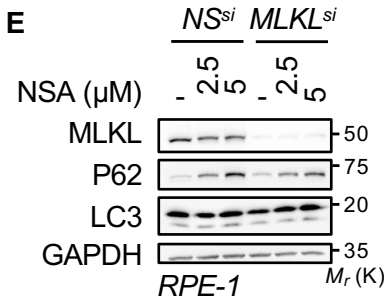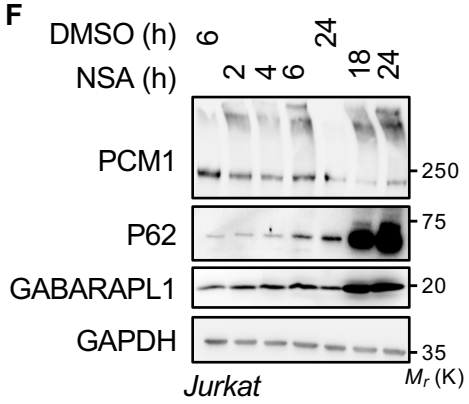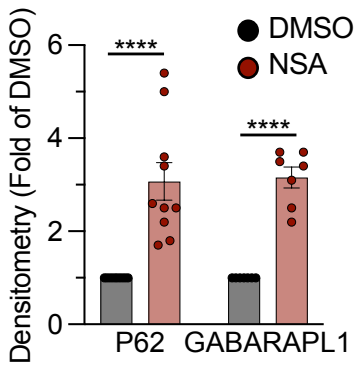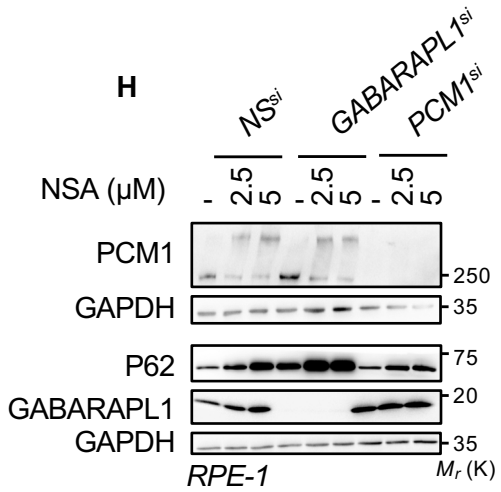
Gene Symbol	Fold Regulation	p-Value
GABARAPL1	5.09	0.023338
SQSTM1 (P62)	2.9	0.028058
MAP1LC3A	2.47	0.01564
MAP1LC3B	2.37	0.003308
CTSD	2.32	0.038429